Journal of Materials Chemistry C

Accepted Manuscript

This article can be cited before page numbers have been issued, to do this please use: A. Yadav, A. K. Srivastava, P. Kulkarni, P. Divya, A. Steiner, B. Praveenkumar and B. Ramamoorthy, *J. Mater. Chem. C*, 2017, DOI: 10.1039/C7TC03375C.

ROYAL SOCIETY OF CHEMISTRY

rsc.li/materials-c

View Article Online
DOI: 10.1039/C7TC03375C

Journal Name

ARTICLE

Anion Induced Ferroelectric Polarization in a Luminescent Metal-organic Cage Compound†

Received 00th January 20xx,
Accepted 00th January 20xx

DOI: 10.1039/x0xx00000x

www.rsc.org/

Ashok Yadav,[a] Anant Kumar Srivastava,[a] Priyangi Kulkarni,[c] Pillutla Divya,[c] Alexander Steiner*[,d], B. Praveenkumar*[,c] and Ramamoorthy Boomishankar*[,a,b]

Metal-organic crystalline solids with ferroelectric properties have attracted significant attention recently as materials for high-tech applications. Here, we describe two crystalline assemblies that contain cationic metal-organic cages $\{[Zn_6(H_2O)_{12}][TPTA]_8\}(NO_3)_{12}\cdot 26H_2O$ (**1**) and $\{[Zn_6(H_2O)_{12}][TPTA]_8\}(ClO_4)_{12}\cdot 18.75H_2O$ (**2**) featuring the tripodal ligand $[PS(NH^3Py)_3]$ (TPTA). Ferroelectric measurement on a single crystal of **1** gave a remnant (P_r) polarization of 1.2 μCcm^{-2} at room temperature. The ferroelectric response originates from the toggling of nitrate anions and solvate molecules found in pockets between the cages. The temperature dependent permittivity of **1** shows an anomalous dielectric peak at 20 °C. This is attributed to the desolvation assisted dielectric relaxation behaviour and signifies the role of solvate molecules in the ferroelectric behaviour of **1**. In addition, this material is highly luminescent exhibiting a bright blue emission under UV-light. This multifunctional behaviour is unique among metal-organic cage frameworks.

Introduction

Ferroelectric (FE) materials exhibit switchable spontaneous polarization in response to an external electric field, which led to a wide range of applications in computing devices, capacitors, micro-electro-mechanical systems (MEMS), field-effect transistors (FETs) and off late as enhanced light absorbing layers in FE photovoltaic cells.[1-11] Ferroelectric crystals that encompass piezoelectric, pyroelectric, luminescent and nonlinear optical properties have shown potential for energy harvesting and multifunctional optoelectronics.[12-25] Rare-earth doped luminescent ferroelectric perovskites are promising candidates for field emission and vacuum fluorescent displays.[26-28] Metal-organic materials with ferroelectric, multiferroic and piezoelectric properties have gained immense interest in recent years[29-38] since they are more amenable for low-temperature fabrication in comparison with traditional ceramic-based materials such as barium titanate and lead zirconate titanate.[39-44] They also offer a broader range of designs and therefore provide a better platform for fine-tuning of material properties. A number of metal tartrates, metal formates, metal sulfates, metal cyanamides and halogenometallates have been screened for ferroelectric and/or multifunctional behaviour.[45-48] In some cases hybrid halogenometallates have shown both ferroelectric and luminescent activity.[49-50] However, synthetic approaches to access molecular materials with ferroelectric properties are still challenging and often serendipitous.

Recently, our group has embarked on a new family of cationic $[Cu^{II}L_2]_n$, $[Ni^{II}L_2]_4$ and $[Co^{II}L_2]_4$ based discrete or polymeric frameworks derived from dipodal phosphoramide ligands of the type $[PhPO(NHPy)_2]$, (Py = 3-pyridyl (^{3}Py) or 4-pyridyl(^{4}Py)), which showed tuned ferroelectric responses depending on the counter anions, dimensionality of the framework and guest molecules present in them.[51-54] Utilizing a similar C_3-symmetric ligand $[PO(NH^3Py)_3]$ (TPPA), Hong and co-workers have synthesized a family of chiral octahedral cages of the type $[M_6L_8]^{12+}$ (point group *O*).[55-56] In order to utilize such chiral cages of high symmetry as frameworks that enable FE behaviour, we paid attention to subtly alter the ligand backbone, counter anions and guest molecules.

Herein, we report an octahedral luminescent cage compound $\{[Zn_6(H_2O)_{12}][TPTA]_8\}(NO_3)_{12}\cdot 26H_2O$ **1**, featuring the tripodal tris(3-aminopyridyl)thiophosphoramide ligand (TPTA),[57] $[PS(NH^3Py)_3]$ which crystallizes in space group *I*4. The ferroelectric measurements on this cage assembly gave a remnant polarization (P_r) value of ~1.2 μCcm^{-2} at room temperature. Polyhedral cages derived from metal-ligand interactions have shown fascinating structures and potential applications in the areas of sorption, sensing, catalysis and host-guest chemistry.[58-68] To the best of our knowledge, this is the first report where framework of a polyhedral cage exhibits

[a] Department of Chemistry, Indian Institute of Science Education and Research (IISER), Pune, Dr. Homi Bhabha Road, Pune – 411008, India. *Email: boomi@iiserpune.ac.in
[b] Centre for Energy Science, Indian Institute of Science Education and Research (IISER), Pune, Dr. Homi Bhabha Road, Pune – 411008, India.
[c] Armament Research and Development Establishment, Dr. Homi Bhabha Road, Pune – 411021, India. *Email: praveenkumar@arde.drdo.in
[d] Department of Chemistry, University of Liverpool, Crown Street, Liverpool – L69 7ZD, United Kingdom. *Email: A.Steiner@liverpool.ac.uk

†Electronic Supplementary Information (ESI) available: [CCDC 968375, 1479696 and 1528473 contains the supplementary crystallographic data. Additional figures and tables pertaining to crystal structures, PXRD, dielectric and ferroelectric measurements]. See DOI: 10.1039/x0xx00000x

View Article Online
DOI: 10.1039/C7TC03775C

not only ferroelectric, but a combination of ferroelectric and luminescent behaviour.

Results and discussion

Syntheses and Structures of the Octahedral Cages

We have found that the solid-state assembly of these metal-organic cages is strongly dependent on the choice of counterion. The treatment of TPTA (Fig. S1-S4, ESI) with $Zn(ClO_4)_2$ resulted in the formation of $\{[Zn_6(H_2O)_{12}][TPTA]_8\}(ClO_4)_{12}\cdot 18.75H_2O$, **2**, which crystallizes in the cubic space group *I*-43d as determined from single crystal X-ray diffraction (SCXRD) and features a racemic mixture of cages; its structure corresponds to that of the TPPA derivative reported by Hong and co-workers.[56] In contrast, use of the nitrate salt $Zn(NO_3)_2\cdot 6H_2O$ led to the formation of $\{[Zn_6(H_2O)_{12}][TPTA]_8\}(NO_3)_{12}\cdot 26H_2O$, **1**, which crystallizes in space group *I*4, consisting of a chiral assembly of cages albeit as part of racemically twinned crystals. The packing of cages in both structures can be described as body-centred; every cage is linked with eight others in a hydrogen-bonded network via water molecules. Both compounds contain partially disordered counterions (Fig. 1, Fig. S5-S9, ESI). However, the disorder of nitrate ions in **1** can give rise to polar assemblies that facilitate a ferroelectric response (as discussed in detail further below); compound **2** does not show this behaviour.

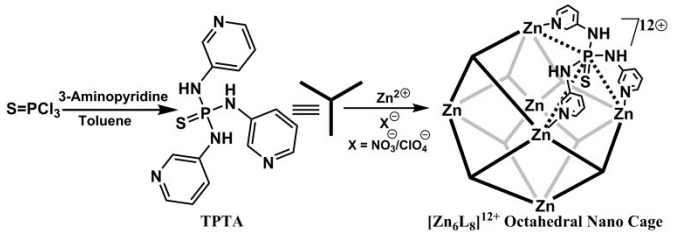

Scheme 1. Schematic diagram showing the formation of octahedral cage assemblies 1 and 2.

Each ligand of the cationic cage $\{[Zn_6(H_2O)_{12}][TPTA]_8\}^{12+}$ is connected to three Zn(II) ions via $N_{pyridyl}$ sites and, in return, each zinc ion displays an octahedral coordination with four equatorial $N_{pyridyl}$ contacts and two water ligands at axial positions (Fig. 1a and Tables S1-S2, ESI). All eight TPTA ligands offer a *syn*-mode of coordination to the Zn^{2+} ions in which the P=S moieties are oriented towards the cavity of the cage. The cages show local chiral octahedral symmetry (point group *O*); the six Zn^{2+} ions are located on the three 4-fold axes and the P and S atoms on the four 3-fold axes (Fig. 1a and 1b). The ligands are all twisted in the same direction around the 3-fold axes. Concomitantly, the square planar ZnN_4 arrangements are also twisted the same way when viewed onto the Zn_6 octahedron.

It is interesting to note that mass spectrometry of aqueous solutions of **1** and **2** indicate the existence of complete cages (Fig. S10, ESI). Variable temperature ^1H and ^{31}P-NMR of **1** and **2** show line broadening at 230 K, which suggest that the cages fluctuate at room temperature but start to freeze into a static conformation at lower temperature (Fig. S11-S14, ESI). Hence, we assume that the cages also freeze upon crystallization to form either chiral (as in **1**) or racemic crystals (as in **2**). Figures 1c and 1d emphasize the chiral and racemic structures of **1** and **2**, by highlighting the relative turns of ZnN_4 squares at the corners of the Zn_6 octahedra.

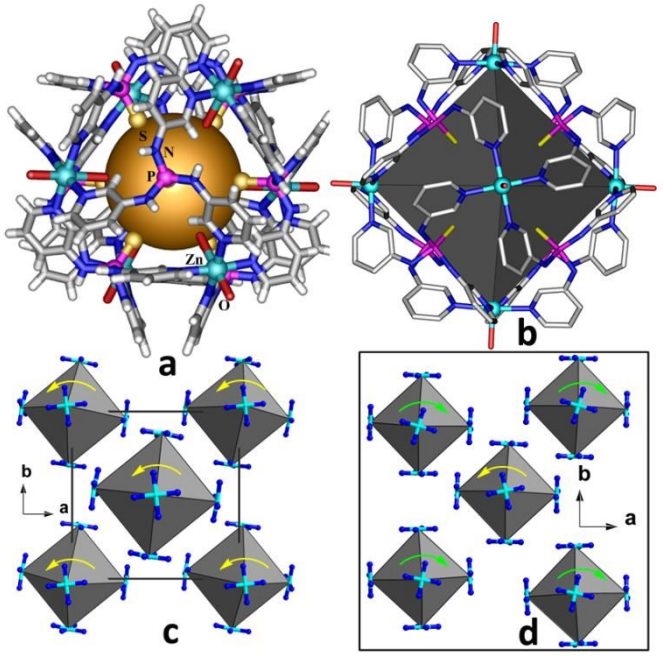

Fig. 1. View of the $\{[Zn_6(H_2O)_{12}][TPTA]_8\}^{12+}$ cage in **1** and **2**; along the 3-fold (a) and 4-fold axis (b). Packing view of the Zn_6 octahedra in **1** (c) and **2** (d) along with the direction of rotation of the ZnN_4 subunits in them. Only a partial segment of the packing in **2** is given; the organic ligands (except those of $N_{pyridyl}$ atoms), anions and solvates are omitted for clarity.

Ferroelectric and Dielectric Studies of 1

Ferroelectric measurements of **1** gave a well saturated hysteresis loop for polarization (P) vs electric field (E) at room temperature characteristic of ferroelectric materials. A closer look at the loop indicates remnant (P_r) and saturation polarization (P_s) values of 1.20 and 0.95 μCcm^{-2}, respectively, at 0.1Hz frequency (Fig. 2a). The slightly higher P_r value as compared to P_s corresponds to the higher relaxation time required for aligning the dipoles created by the weak hydrogen bonding interactions. Such a behaviour has also been observed in several supramolecular ferroelctric systems such as TGS.[69] The obtained E_c value of 0.86 $kVcm^{-1}$ is considerably low which indicates the facile switching of the ferroelectric domains in **1**. Recording the data at 1Hz frequency gave an almost similar P-E loop with a P_r of 1.09 μCcm^{-2} and E_c of 1.40 $kVcm^{-1}$ (Fig. S15, ESI). The plot of leakage current vs. applied field shows a very low leakage current of the order of 10^{-7} A and exhibits peaks corresponding to the domain switching at the coercive field which confirms the ferroelectric origin of the obtained loop (Fig. 2b). To further probe its non-conducting behaviour, the crystals of **1** (with contacts) were directly subjected to a dc electric field. The output current measured in this experiment was found to be very low (47.16 μA) when 1kV of dc voltage

was passed through the crystal. This confirms the resistive nature of the crystal (Table S3, ESI).

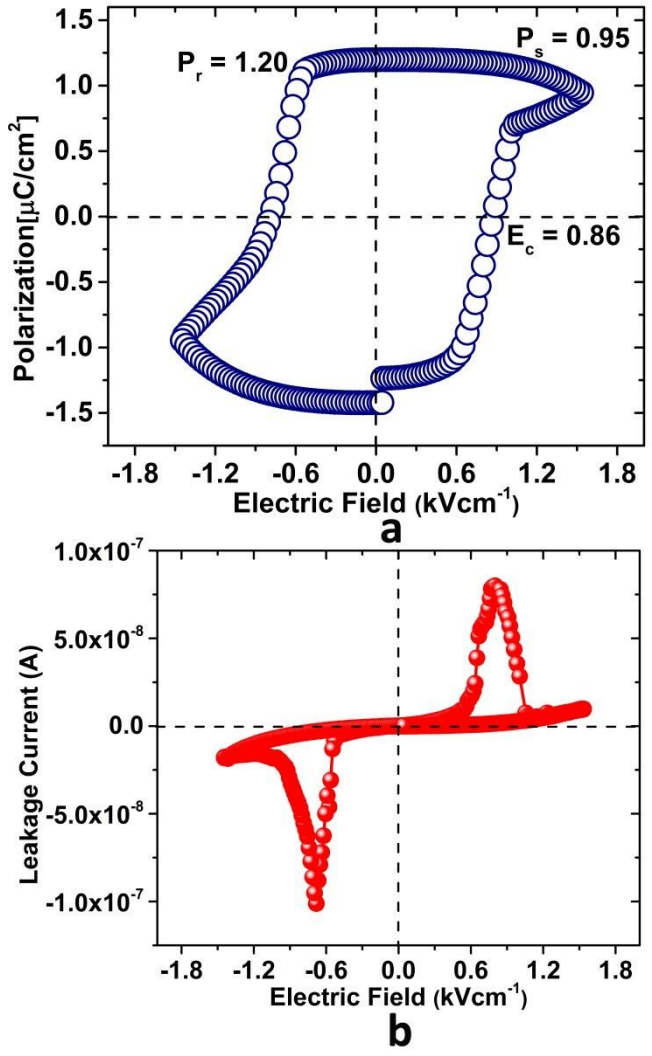

Fig. 2. (a) Ferroelectric hysteresis loop for **1** and (b) the corresponding plot of the leakage current vs. voltage.

In contrast, a similar P-E loop measurement for **2** gave a negligible polarization (Fig. S16, ESI). The obtained P_r values for **1** are in good comparison with several polymeric, organic and molecular ferroelectric materials (Table S4, ESI).[70] Furthermore, ferroelectric fatigue measurements were performed on **1** (at 1 Hz) to check the loss of remnant polarization during bipolar switching cycles. These measurements showed the retention of nearly 50% of the polarization and rectangularity of the loop after 10^5 switching cycles (Fig. S17, ESI).

As described earlier, the cages themselves, as well as the framework they build have no dipole moment due to the octahedral symmetry of the cage. The polarization necessary for the ferroelectric response originates from the distribution of nitrate ions relative to the framework and its interactions with the solvate molecules of water (Fig. S18-S19, ESI). The network of nitrate ions and water molecules in **1** consists of both ordered and disordered parts. The ordered part contains one nitrate ion and four water molecules which form bridges between adjacent exogenically facing $P(NH)_3$ ligand segments (Fig. 3a). As such all eight $P(NH)_3$ units of a given cage are connected in this way to $P(NH)_3$ units of neighbouring cages. The disordered parts consist of four nitrate ions and water molecules that are located in isolated pockets created by the packing of the cages. These ions are disordered over two positions which are crystallographically related by the 2-fold axis that runs parallel to the *c*-axis (Wyckoff site 4b in space group *I*4). Switching between the two disordered sites would involve a movement of ions along the a- and b-axis, respectively (Fig. 3b).

Measurements of capacitance C_p (directly proportional to ε) on individual single crystals show that the dipole moments in **1** were dominant along the a- and b- and weaker along the c-axis (Table S5, ESI). In a fully polarized state, the location of nitrate ions will be biased towards one of the two positions. A similar bias could also be shown by the disordered solvate molecules perpendicular to the c-axis. If the crystal was fully polarized, the space group symmetry would be reduced to *I*1 (*P*1) due to the absence of both 2-fold and 4-fold axes. Refinement of the structure of freshly prepared crystals of **1** in the lower symmetry *I*1 revealed the same disorder as observed for *I*4. This indicates that bulk polarization does not occur prior to the application of an electric field (Fig. 3c).[71] Thus, one can assume that the toggling of nitrate anions and water molecules within the isolated pockets of the crystal structure plays a role in the polarisation.

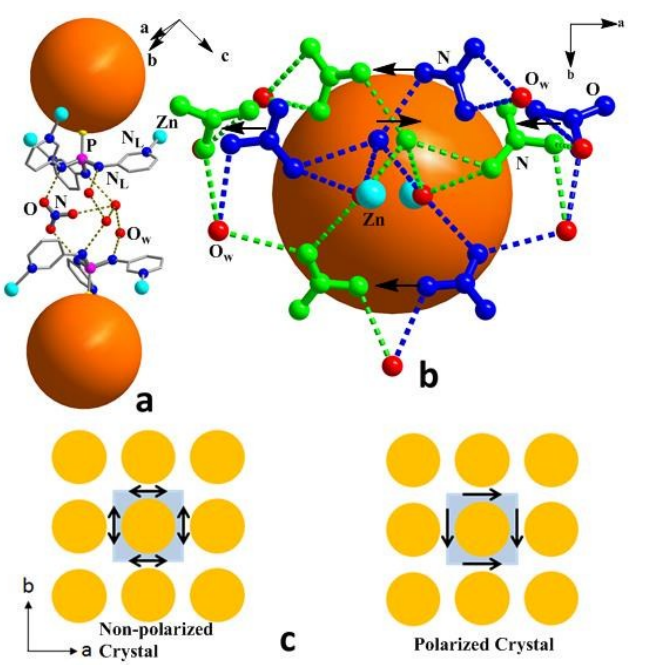

Fig. 3. Segments of the (a) ordered and (b) disordered parts of the nitrate anions and their H-bonding interactions. The two disordered parts are shown in blue and green colours and the arrows indicate the possible migration pathways. The octahedral cage core is depicted as an orange coloured sphere. (c) Schematic diagram showing the overall arrangement of dipoles in the structure of **1** before and after polarization (cages are shown in orange).

View Article Online
DOI: 10.1039/C7TC03375C

To further investigate the polarization attributes of **1**, we performed dielectric permittivity (ε) measurements. From the plot of the real part of dielectric permittivity (ε') as a function of frequency it can be noted that the maximum room temperature ε' value is 39.4 at 100 Hz (Fig. S20-S21, ESI). These values gradually decreased at higher frequencies indicating the contribution of all polarization mechanisms at lower frequencies.[51] The computed dipole moment for **1** gave a value of 59.4 D which is consistent with its observed high-dielectric constant. Next, we studied the temperature dependence of dielectric permittivity at various frequencies between 10^2 and 10^6 Hz. These curves show a broad feature for all measured frequencies with an increase in permittivity up to room temperature (onset at -50 °C), beyond which it gradually decreases attaining a minimum value of around 8-10 at 60 °C (Fig. 4a). The maximum ε' value of 39.4, which corresponds to an anomalous dielectric peak, is observed at 20 °C at 100 Hz. Furthermore, the intensity of the anomalous peak gradually declined and slightly shifted at higher frequencies suggesting the presence of dielectric relaxation behaviour in **1**. These observations suggest that the dielectric anomaly in **1** is due to desolvation (see also below). Furthermore, the dielectric loss (tan δ) observed at various frequencies are very low indicating the high dielectric and ferroelectric nature of **1** (Fig. 4b).

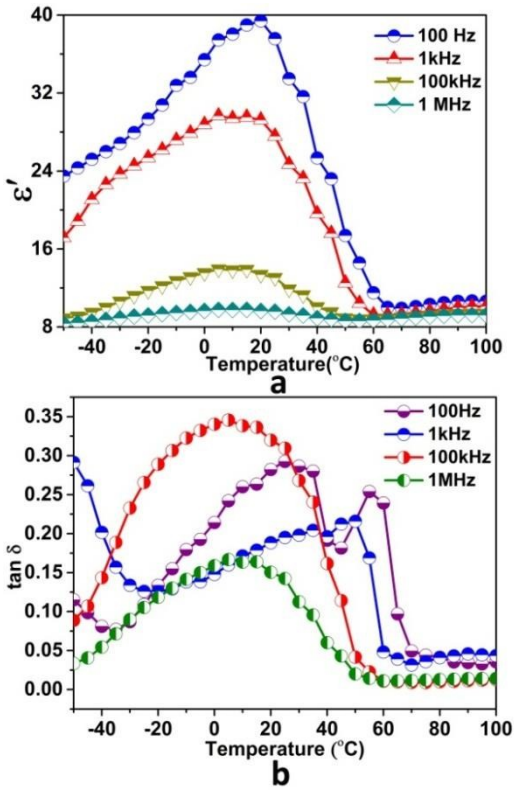

Fig. 4. Plots of (a) the real part of dielectric permittivity and (b) the dielectric loss as a function of temperature.

The structural integrity of **1** and the desolvation dependant dielectric anomaly has been confirmed by thermogravimetric-differential thermal analysis, infrared spectra recorded in the ATR mode, variable temperature powder X-ray diffraction analysis, SCXRD experiments on **1** at various temperatures between -173 and 100 °C and solid state CP-MAS ^{31}P-NMR spectra. The thermogravimetric-differential thermal analysis of **1** gave an irreversible endothermic peak at 30 °C indicating the onset of desolvation at the transition temperature (Fig. S24-S26, ESI). The Fourier-transform infrared spectra recorded in the ATR mode for the neat samples of **1**, $\mathbf{1}_{desolvated}$ and $\mathbf{1}_{resolvated}$ gave almost similar peak patterns except that the –OH stretching frequencies due to the solvate molecules were absent in the case of $\mathbf{1}_{desolvated}$ (Fig. 5a).

The variable temperature powder X-ray diffraction (VTPXRD) analysis showed that the peak patterns begin to change at 30 °C and the profile obtained after 120 °C matched with that of $\mathbf{1}_{desolvated}$ (Fig. S27, ESI). However, the PXRD of $\mathbf{1}_{resolvated}$ exactly matched with that of the as-made **1** confirming the desolvation and resolvation processes in **1** are reversible (Fig. 5b). The SCXRD experiments performed on **1** at various temperatures between -173 and 100 °C are in agreement with the VTPXRD data. Also, a crude model for the structure of **1** at both 273 and 295 K have been obtained that confirms the same packing of cages in *I*4 and even obtained a reflection pattern at 323 K which shows similar unit cell parameters (Fig. S28, Table S6, ESI). This confirms that the integrity of the crystal is retained even after crossing the T_c. The solid state CP-MAS ^{31}P-NMR spectra of the bulk samples of **1**, $\mathbf{1}_{desolvated}$ and $\mathbf{1}_{resolvated}$ gave almost identical peak patterns consisting of a sole signal due to ligand phosphorus atom at 39.13 ppm (Fig. S29, ESI).

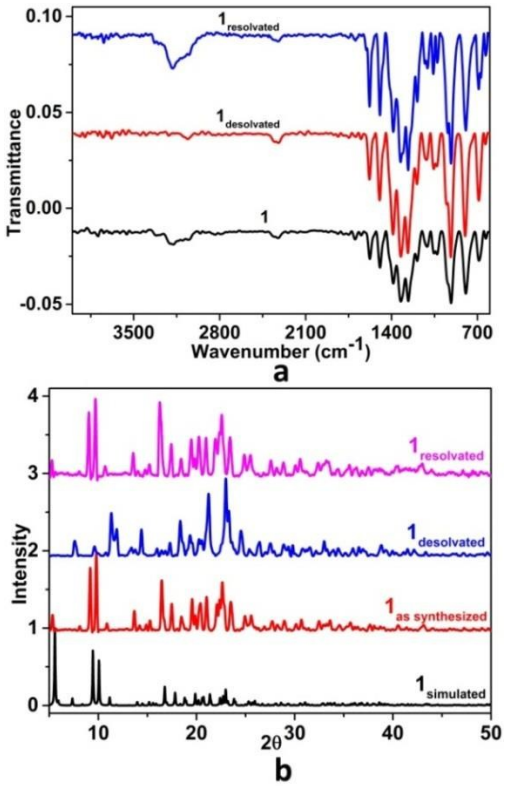

Fig. 5. (a) IR spectra for **1**, $\mathbf{1}_{desolvated}$, and $\mathbf{1}_{resolvated}$. (b) PXRD pattern of **1** at various states.

Optical Properties of 1

It is worth noting that the framework of cages in **1**, which can be regarded as static during the ferroelectric response, is polar in itself (space group *I*4). The direction of the ferroelectric response, on the other hand, lies orthogonal to the polar 4-fold axis, leading to an overall reduction in symmetry to *I*1. Hence, the extra 'permanent' polarity orthogonal to the direction of ferroelectricity implies further interesting properties. Preliminary non-linear optical measurements (NLO) were obtained for **1** in both solvated and desolvated states. The second harmonic generation (SHG) intensities for the bulk un-sieved samples of **1**, $\mathbf{1}_{desolvated}$ and $\mathbf{1}_{resolvated}$ were found to be around 30, 20 and 32 %, respectively, with respect to the standard urea sample (Table S7, ESI). The cage assembly of **1** was also found to exhibit bright blue luminescence under UV-light in the solid state owing to intra-ligand (π-π*) transitions (Figure 6). The emission spectrum of **1** shows an intense band at λ_{em} = 398 nm (λ_{ex} = 345 nm).[72] The decay profile recorded on **1** gave a lifetime of 6.9 ns for this fluorescence emission (Fig. S31, ESI). Observation of such dual properties (fluorescence and ferroelectricity) promises interesting applications of metal-organic materials for future electro-optical and energy harvesting applications.

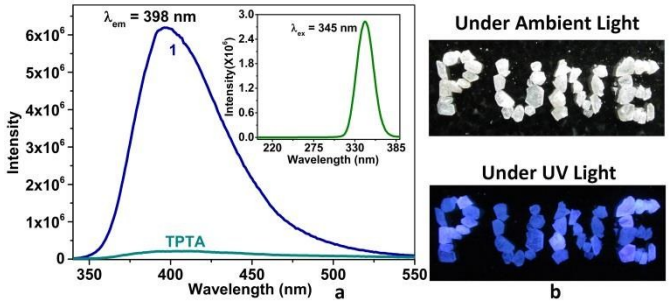

Fig. 6. (a) Fluorescence profile of **1** and TPTA in the solid state; the inset shows the excitation spectrum of **1**. (b) View of the crystals of **1** at ambient and under UV light

Conclusions

In conclusion, this work demonstrates that by subtly altering the molecular constituents of a metal-ligand cage assembly, it is possible to derive materials with ferroelectric properties. An assembly of $\{[Zn_6(H_2O)_{12}][TPTA]_8\}^{12+}$ cages and nitrate ions gave a ferroelectric remnant polarization value of 1.2 μCcm^{-2} at room temperature. The polarization can be attributed to the toggling of anions and water molecules that are located in pockets between the cages. Further, dielectric measurements showed that **1** exhibits a desolvation assisted dielectric transition associated with the release of solvate molecules from the unit cell packing. In addition, crystals of **1** are noncentrosymmetric, which gives rise to NLO activity. Furthermore, the compound **1** is highly luminescent showing a bright blue emission under UV-light. Such multifunctional behaviour is unique among metal-organic cage compounds and may pave the way for new and interesting applications.

Acknowledgements

View Article Online
DOI: 10.1039/C7TC03375C

This work was supported by SERB, India via Grant No. EMR/2016/000614 (R.B.). A.Y. and A.K.S. thank the CSIR, India for the fellowship. We thank Dr. S. Nair and S. Panja for help with electrical measurements.

References

1 M. E. Lines and A. M. Glass, *Principles and applications of ferroelectrics and related materials*, Oxford university press, 1977.
2 C. A. P. Dearaujo, J. D. Cuchiaro, L. D. Mcmillan, M. C. Scott and J. F. Scott, *Nature*, 1995, **374**, 627-629.
3 T. A. Vanderah, *Science*, 2002, **298**, 1182-1184.
4 H. N. Lee, H. M. Christen, M. F. Chisholm, C. M. Rouleau and D. H. Lowndes, *Nature*, 2005, **433**, 395-399.
5 G. Rijnders and D. H. Blank, *Nature*, 2005, **433**, 369-370.
6 J. F. Scott, *Science*, 2007, **315**, 954-959.
7 K. Uchino, *Ferroelectric Devices 2nd Edition*, CRC press, 2009.
8 S. T. Han, Y. Zhou and V. Roy, *Adv. Mater.*, 2013, **25**, 5425-5449.
9 J. F. Scott, *Ferroelectric memories*, *Springer Science & Business Media*, 2013.
10 Y. Xu, *Ferroelectric materials and their applications*, Elsevier, 2013.
11 E. Salje and J. F. Scott, *Appl. Phys. Lett.*, 2014, **105**, 252904.
12 N. A. Spaldin and M. Fiebig, *Science*, 2005, **309**, 391-392.
13 W. Eerenstein, N. Mathur and J. F. Scott, *Nature*, 2006, **442**, 759-765.
14 K. M. Ok, E. O. Chi and P. S. Halasyamani, *Chem. Soc. Rev.*, 2006, **35**, 710-717.
15 A. K. Cheetham and C. N. R. Rao, *Science*, 2007, **318**, 58-59.
16 S.-W. Cheong and M. Mostovoy, *Nat. Mater*., 2007, **6**, 13-20.
17 Z. Hu, M. Tian, B. Nysten and A. M. Jonas, *Nat. Mater.*, 2009, **8**, 62-67.
18 R. Ramesh, *Nature*, 2009, **461**, 1218-1219.
19 J. Zhang, B. Xiang, Q. He, J. Seidel, R. Zeches, P. Yu, S. Yang, C. Wang, Y. Chu and L. Martin, *Nat. Nanotechnol*., 2011, **6**, 98-102.
20 W. Zhang and R.-G. Xiong, *Chem. Rev.*, 2011, **112**, 1163-1195.
21 D.-W. Fu, H.-L. Cai, Y. Liu, Q. Ye, W. Zhang, Y. Zhang, X.-Y. Chen, G. Giovannetti, M. Capone and J. Li, *Science*, 2013, **339**, 425-428.
22 C. Bowen, H. Kim, P. Weaver and S. Dunn, *Energ. Environ. Sci.*, 2014, **7**, 25-44.
23 A. S. Tayi, A. Kaeser, M. Matsumoto, T. Aida and S. I. Stupp, *Nat. Chem.*, 2015, **7**, 281-294.
24 Y. Tian, A. Stroppa, Y. S. Chai, P. Barone, M. Perez-Mato, S. Picozzi and Y. Sun, *physica status solidi (RRL)-Rapid Research Letters*, 2015, **9**, 62-67.
25 C. R. Bowen, V. Y. Topolov and H. A. Kim, Springer, 2016.
26 P. Diallo, P. Boutinaud, R. Mahiou and J. Cousseins, *Physica Status Solidi-A-Applied Research*, 1997, **160**, 255-264.
27 H. Yamamoto and S. Okamoto, *Displays*, 2000, **21**, 93-98.
28 H. Yamamoto, S. Okamoto and H. Kobayashi, *J. lumin.*, 2002, **100**, 325-332.
29 Q. Ye, Y.-M. Song, G.-X. Wang, K. Chen, D.-W. Fu, P. W. Hong Chan, J.-S. Zhu, S. D. Huang and R.-G. Xiong, *J. Am. Chem. Soc.*, 2006, **128**, 6554-6555.
30 H.-Y. Ye, D.-W. Fu, Y. Zhang, W. Zhang, R.-G. Xiong and S. D. Huang, *J. Am. Chem. Soc.*, 2008, **131**, 42-43.
31 P. Jain, V. Ramachandran, R. J. Clark, H. D. Zhou, B. H. Toby, N. S. Dalal, H. W. Kroto and A. K. Cheetham, *J. Am. Chem. Soc.*, 2009, **131**, 13625-13627.
32 W. Zhang, H.-Y. Ye and R.-G. Xiong, *Coord. Chem. Rev.*, 2009, **253**, 2980-2997.

33 G. Rogez, N. Viart and M. Drillon, *Angew. Chem. Int. Ed*., 2010, **49**, 1921-1923.
34 T. Hang, W. Zhang, H.-Y. Ye and R.-G. Xiong, *Chem. Soc. Rev.*, 2011, **40**, 3577-3598.
35 A. Stroppa, P. Jain, P. Barone, M. Marsman, J. M. Perez-Mato, A. K. Cheetham, H. W. Kroto and S. Picozzi, *Angew. Chem.*, 2011, **123**, 5969-5972.
36 A. Stroppa, P. Barone, P. Jain, J. M. Perez-Mato and S. Picozzi, *Adv. Mater.*, 2013, **25**, 2284-2290.
37 Y. Tian, A. Stroppa, Y. Chai, L. Yan, S. Wang, P. Barone, S. Picozzi and Y. Sun, *Scientific Reports*, 2014, **4**.
38 Y. Zhang, H. Y. Ye, D. W. Fu and R. G. Xiong, *Angew. Chem.*, 2014, **126**, 2146-2150.
39 R. Ramesh, J. Lee, T. Sands, V. Keramidas and O. Auciello, *Appl. Phys. Lett.*, 1994, **64**, 2511-2513.
40 G. H. Haertling, *J. Am. Ceram. Soc.*, 1999, **82**, 797-818.
41 B. Park, B. Kang, S. Bu, T. Noh, J. Lee and W. Jo, *Nature,* 1999, **401**, 682-684.
42 Y. Saito, H. Takao, T. Tani, T. Nonoyama, K. Takatori, T. Homma, T. Nagaya and M. Nakamura, *Nature*, 2004, **432**, 84-87.
43 X. Long and Z.-G. Ye, *Chem. Mater.*, 2007, **19**, 1285-1289.
44 J. Zylberberg, A. A. Belik, E. Takayama-Muromachi and Z.-G. Ye, *Chem. Mater.*, 2007, **19**, 6385-6390.
45 P. Jain, N. S. Dalal, B. H. Toby, H. W. Kroto and A. K. Cheetham, *J. Am. Chem. Soc.*, 2008, **130**, 10450-10451.
46 G.-C. Xu, X.-M. Ma, L. Zhang, Z.-M. Wang and S. Gao, *J. Am. Chem. Soc.*, 2010, **132**, 9588-9590.
47 G.-C. Xu, W. Zhang, X.-M. Ma, Y.-H. Chen, L. Zhang, H.-L. Cai, Z.-M. Wang, R.-G. Xiong and S. Gao, *J. Am. Chem. Soc.*, 2011, **133**, 14948-14951.
48 D. Di Sante, A. Stroppa, P. Jain and S. Picozzi, *J. Am. Chem. Soc.*, 2013, **135**, 18126-18130.
49 Y. Zhang, W. Q. Liao, D. W. Fu, H. Y. Ye, C. M. Liu, Z. N. Chen and R. G. Xiong, *Adv. Mater.*, 2015, **27**, 3942-3946.
50 Y. Zhang, W.-Q. Liao, D.-W. Fu, H.-Y. Ye, Z.-N. Chen and R.-G. Xiong, *J. Am. Chem. Soc.*, 2015, **137**, 4928-4931.
51 A. K. Srivastava, B. Praveenkumar, I. K. Mahawar, P. Divya, S. Shalini and R. Boomishankar, *Chem. Mater.*, 2014, **26**, 3811-3817.
52 A. K. Srivastava, P. Divya, B. Praveenkumar and R. Boomishankar, *Chem. Mater.*, 2015, **27**, 5222-5229.
53 A. K. Srivastava, T. Vijayakanth, P. Divya, B. Praveenkumar, A. Steiner and R. Boomishankar, *J. Mater. Chem. C*, 2017, **5**, 7352-7359.
54 R. Boomishankar and A. K. Srivastava, *Phosphorus, Sulfur, and Silicon and the Related Elements*, 2016, **191**, 618-623.
55 N. Li, F. Jiang, L. Chen, X. Li, Q. Chen and M. Hong, *Chem. Commun.*, 2011, **47**, 2327-2329.
56 X.-J. Li, F.-L. Jiang, M.-Y. Wu, S.-Q. Zhang, Y.-F. Zhou and M.-C. Hong, *Inorg. Chem.*, 2012, **51**, 4116-4122.
57 A. Yadav, M. S. Deshmukh and R. Boomishankar, *J. Chem. Sci.*, 2017, **129**, 1093-1103.
58 Y. Inokuma, T. Arai and M. Fujita, *Nat. Chem.*, 2010, **2**, 780-783.
59 R. Chakrabarty, P. S. Mukherjee and P. J. Stang, *Chem. Rev.*, 2011, **111**, 6810-6918.
60 N. Ahmad, H. A. Younus, A. H. Chughtai and F. Verpoort, *Chem. Soc. Rev.*, 2015, **44**, 9-25.
61 Q. Gan, T. K. Ronson, D. A. Vosburg, J. D. Thoburn and J. R. Nitschke, *J. Am. Chem. Soc.*, 2015, **137**, 1770-1773.
62 A. K. Gupta, A. Yadav, A. K. Srivastava, K. R. Ramya, H. Paithankar, S. Nandi, J. Chugh and R. Boomishankar, *Inorg. Chem.*, 2015, **54**, 3196-3202.
63 60. X. Jing, C. He, Y. Yang and C. Duan, *J. Am. Chem. So.c*, 2015, **137**, 3967-3974.
64 U. Stoeck, I. Senkovska, V. Bon, S. Krause and S. Kaskel, *Chem. Commun.*, 2015, **51**, 1046-1049.
65 H. Vardhan and F. Verpoort, *Adv. Synth. Catal.*, 2015, **357**, 1351-1368.
66 C. Wang, J. Shang, Y. Lan, T. Tian, H. Wang, X. Chen, J. Y. Gu, J. Z. Liu, L. J. Wan and W. Zhu, *Adv. Funct. Mater.*, 2015, **25**, 6009-6017.
67 Q. G. Zhai, C. Mao, X. Zhao, Q. Lin, F. Bu, X. Chen, X. Bu and P. Feng, *Angew. Chem. Int. Ed.*, 2015, **54,** 7886-7890.
68 H. Vardhan, M. Yusubov and F. Verpoort, *Coord. Chem. Rev.*, 2016, **306**, 171-194.
69 H. Ma, W. Gao, J. Wang, T. Wu, G. Yuan, J. Liu and Z. Liu, *Adv. Electron. Mater.*, 2016, **2**, 1600038.
70 S. Horiuchi and Y. Tokura, *Nat. Mater.*, 2008, **7**, 357-366.
71 T. Akutagawa, H. Koshinaka, D. Sato, S. Takeda, S.-I. Noro, H. Takahashi, R. Kumai, Y. Tokura and T. Nakamura, *Nat. Mater.*, 2009, **8**, 342-347.
72 For **2**, the λ_{em} was found to be 393 nm (Figure S30).

View Article Online
DOI: 10.1039/C7TC03375C

Graphical Abstract

Anion Induced Ferroelectric Polarization in a Luminescent Metal-organic Cage Compound

Ashok Yadav, Anant Kumar Srivastava, Priyangi Kulkarni, Pillutla Divya, Alexander Steiner,* B. Praveenkumar,* and Ramamoorthy Boomishankar*

A cage assembly consisting of an axially symmetric nonpolar octahedral [Zn_6L_8] core exhibits an interesting multifunctional luminescence and ferroelectric order at room temperature. The ferroelectric response originates from the toggling of nitrate anions and solvate molecules found in pockets between the cages.